ISSN 0036-0236, Russian Journal of Inorganic Chemistry, 2021, Vol. 66, No. 12, pp. 1802–1810. © Pleiades Publishing, Ltd., 2021.
Russian Text © The Author(s), 2021, published in Zhurnal Neorganicheskoi Khimii, 2021, Vol. 66, No. 12, pp. 1684–1692.

Textured Barium Hexaferrite Films on Silicon Substrates with Aluminum Oxide and Titanium Oxide Barrier Layers

V. G. Kostishin[a], A. Yu. Mironovich[a, *], A. V. Timofeev[a], R. I. Shakirzyanov[a], I. M. Isaev[a], A. V. Sorokin[b], and A. I. Ril'[c]

[a] *National University of Science & Technology "MISiS," Moscow, 119049 Russia*
[b] *Moscow Plant "Sapfir," Moscow, 117545 Russia*
[c] *Kurnakov Institute of General and Inorganic Chemistry, Russian Academy of Sciences, Moscow, 119991 Russia*
**e-mail: amironovich24@gmail.ru*

Received April 8, 2021; revised May 28, 2021; accepted May 31, 2021

Abstract—The possibility of synthesizing textured barium hexaferrite films on silicon wafers with Ti, Al_2O_3/Ti, or Al_2O_3/TiO_2 barrier layers was studied. X-ray diffraction (XRD) showed that, after crystallization annealing, the hexaferrite phase with the (00l) preferred orientation was formed only when there was contact between $BaFe_{12}O_{19}$ and Al_2O_3. The hexaferrite microstructure in these samples, according to atomic force microscopy (AFM), is represented by rounded grains, which are typical of films where the hexagonal axis is perpendicular to the surface plane. Titanium in a $BaFe_{12}O_{19}$/Al_2O_3/Ti sample was partially oxidized during the synthesis. This process and the associated phase transformations in TiO_2 are assumed to induce mechanical stress in the structure and, as a consequence, the formation of macroscopic defects (bulges). Complete pre-oxidation of the titanium film produced a textured $BaFe_{12}O_{19}$ structure without macroscopic defects.

Keywords: crystallographic texture, thin films, barium hexaferrite, rutile, brookite, aluminum titanate, aluminum oxide

DOI: 10.1134/S0036023621120093

INTRODUCTION

$BaFe_{12}O_{19}$ (BaM) and $SrFe_{12}O_{19}$ (SrM) are of the greatest practical importance among the hexagonal ferrites (HFs); they are widely used in microwave and radio engineering, communication systems, and as permanent magnets [1, 2]. The value of these ferrites is due to the unique combination of their properties: high magnetic and dielectric constants, low conductivity, high constants of uniaxial crystallographic anisotropy, resistance to mechanical stress, and chemical stability [1, 3]. BaM and SrM have long been known and well studied. Nevertheless, interest in hexaferrites does not fade over the years, for there are many ways to modify these materials. For example, modifying of the chemical composition through isomorphic substitution of cations makes it possible, to some extent, to tune the main magnetic parameters of HFs [4–8]. At the same time, the properties and characteristics of HFs can change upon the transition of the material to alternative states, to nanopowders [9, 10] or thin films [11].

The topicality of preparation of HFs in thin films is in the general trend toward the miniaturization of electronic devices and the advent of planar technology. For ferrite-based nonreciprocal microwave devices, the weight–size parameters are mostly associated with the presence of external permanent magnets, which provide offset fields. Theoretically, these magnets can be eliminated using the self-biased effect, which is possible in textured HF films due to their high constants of uniaxial crystallographic anisotropy [12].

The preparation of anisotropic HF films is associated with certain difficulties, for the material is required to have a high degree of crystallographic texture. Liquid phase epitaxy has reached acceptable results [13], but this method is relatively complex and economically impractical. More facile and low-cost methods of synthesis (sol–gel [14–16] and screen printing [17, 18]) do not yet provide a high degree of texture in samples. Vacuum deposition techniques (pulsed laser deposition [19] and ionic sputtering [20]) have a potential for producing quality anisotropic films. The specifics of implementation of these techniques for HF preparation have been surveyed [21].

The choice of substrate is a matter of special importance in the preparation of thin films. (00l) single-crystal sapphire wafers [22] or Pt(111)/SiO_2/Si structures [23] are used for the production of HFs with the easy magnetization axis directed perpendicular to the surface plane. (00l)-Oriented HF growth occurs in the epitaxial mode. However, there is another approach to the growth of the (00l) texture. Metals

with FCC lattices are known to grow with the (111) texture on amorphous surfaces; this is due to the nuclei of this orientation having the least surface energy and the absence of contributions from stresses generated by the misfit of film and substrate lattice parameters [24]. In turn, minimization of the surface energy is due to the closest packing of atoms [25]. A similar mechanism is intrinsic to hexaferrites and manifests itself in the spontaneous formation of the (00l) texture [26, 27]. The use of this phenomenon, obviously, helps to reduce the cost of production and research of anisotropic HF films.

There are only few works on the growth of oriented BaM films on amorphous surfaces [26, 27]. Perhaps this is due to the inapplicability of silicon dioxide, the most common amorphous material, in thin-film technology. It is known that silicon diffuses from the substrate into the film [28], which can lead to the formation of silicate phases [28, 29] and misalignment of HF grains. Thus, this growth technique requires materials that are highly chemically inert over a wide temperature range.

Given this situation, in our previous work we attempted to manufacture anisotropic $BaFe_{12}O_{19}$ films on amorphous Si_3N_4 [30]. Although a highly textured HF phase was formed, the material was found unsuitable for practical use due to macroscopic blistering and violation of integrity after crystallization annealing. Attempts to find references to such defects in hexaferrite films in the literature were unsuccessful. Nevertheless, similar bulges were repeatedly observed in films of other materials and assigned to the effect of strong mechanical stresses [31]. Stress control processes in films are quite complex, involve the use of expensive equipment, and are poorly applicable to amorphous and textured materials [31]. In this regard, it is difficult to recognize unambiguously and reliably and eliminate stress sources in the prepared samples. However, silicon nitride films are well known for their strong internal or residual stresses [32], which substantially depend on the synthesis conditions [33]. The nature of the defects implies that the stresses in the resulting films were compressive stresses. Therefore, a layer of amorphous Al_2O_3 was added to the structure, the stresses in which caused tension to compensate for the compression in $BaFe_{12}O_{19}/Si_3N_4$. The result of this was a defect-free anisotropic HF film.

Despite the positive result [30], research in this direction should be continued in order to find a substitute for Si_3N_4. As mentioned above, this material is too sensitive to synthesis conditions, which negatively affects the reproducibility of its properties (film thickness and stress values). In addition, its preparation process (chemical vapor deposition) requires special equipment and hazardous reagents. Therefore, the search for a more facile alternative can be considered a topical task.

In this work, we studied the usefulness of titanium and its natural oxide as one of the barrier layers for growing textured BaM films. Metallic titanium in its low-temperature polymorph has a hexagonal lattice with the [001] close packing direction; accordingly, the (00l) preferred grain orientation is often observed in titanium films [34], and the HF can potentially inherit it. Titanium films can be easily manufactured using equipment intended for the preparation of $BaFe_{12}O_{19}$ films by physical vapor deposition.

EXPERIMENTAL

The substrates used were (001) single-crystal silicon wafers. At the first stage, BaM/Ti/Si and BaM/Al_2O_3/Ti/Si samples were manufactured, and at the second, BaM/Al_2O_3/TiO_2/SiO_2/Si and BaM/Al_2O_3/TiO_2/Si were manufactured. Silicon was oxidized to SiO_2 (1100°C, 1 h) and titanium was oxidized to TiO_2 (900°C, 3 h) in air inside a muffle furnace. Al_2O_3 (~200 nm), $BaFe_{12}O_{19}$ (~100 nm), and Ti (~100 nm) films were prepared by ion beam sputtering. The targets used were a polycore Al_2O_3 wafer, a Ti disk, and a stoichiometric $BaFe_{12}O_{19}$ tablet manufactured by standard ceramic technology. Before films were applied, the substrates were sonicated with isopropyl alcohol and washed with distilled water. Then, the substrates were placed at a distance of about 35 mm from the target in the vacuum chamber of a UVN-71 setup. During deposition, the discharge current of the ion source was 40 mA, the discharge voltage was 2 kV, and the working gas (Ar) pressure was maintained at 3×10^{-4} Torr. Substrates were heated to 310 ± 10°C to improve adhesion and remove adsorbed gases. Hexaferrite deposition was followed by crystallization annealing in air for 1 h at 900°C (the heating rate was 300 K/h). The thickness of the films was measured on a DekTak 150 contact profilometer, in the case of transparent coatings, on an LEF-3M-1 ellipsometer. X-ray diffraction (XRD) patterns were obtained on a Bruker D8 ADVANCE diffractometer (CuK_α radiation, $\lambda = 0.154$ nm, $U = 40$ kV, $I = 40$ mA). The angular step was 0.02°; the 2θ angle range was 15°–100°. The surface morphology of films was studied by atomic force microscopy (AFM) using an NT-MDT NTEGRA Prima scanning probe microscope.

RESULTS AND DISCUSSION

The AFM micrographs and optical images of the surface of BaM/Ti/Si and BaM/Al_2O_3/Ti/Si samples are shown in Fig. 1. The BaM film on Al_2O_3/Ti/Si consists of rounded grains; it is rare that hexagonal faceting can be discerned in crystallites. This morphology, which is typical of the (00l) hexaferrite texture, has been repeatedly observed previously [23, 30]. Gaps between crystallites are well distinguishable. In the BaM film on Ti/Si, the grains are arranged more

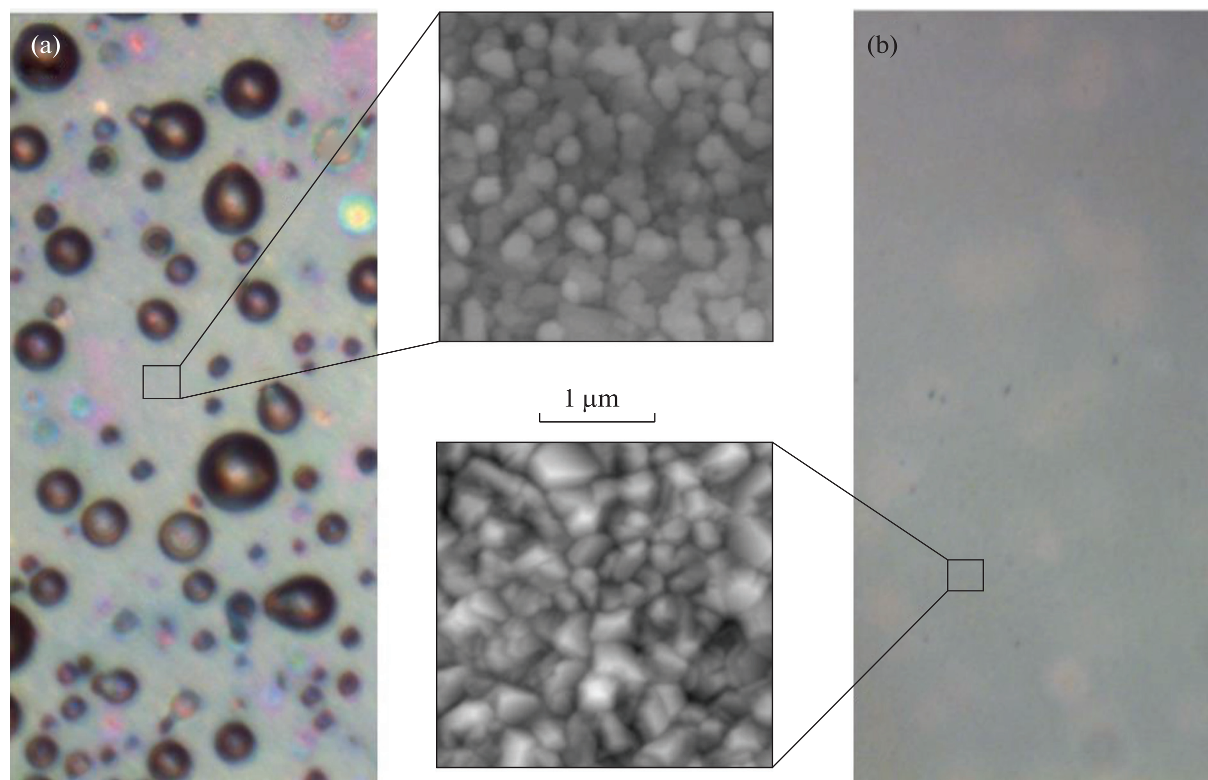

Fig. 1. Optical images (×20) and AFM images of (a) BaM/Al_2O_3/Ti/Si and (b) BaM/Ti/Si samples.

densely, their faces are more distinct, but the morphology and orientation indicate the absence of texture.

The BaM/Al_2O_3/Ti/Si surface is coated by bulges, which negatively affects the usefulness of films. BaM/Ti/Si films have no such surface defects, but contrasting areas stand out from the general view. Due to their round shapes and commensurateness to the defects observable on Fig. 1a, we may assume that these areas are a kind of swelling nuclei.

The XRD patterns of BaM/Ti/Si and BaM/Al_2O_3/Ti/Si are shown in Fig. 2, and the indexes of planes corresponding to the identified reflections appear in Table 1.

The XRD pattern of the BaM/Al_2O_3/Ti/Si sample features strong (00l) peaks of barium hexaferrite, in match with the AFM results. In addition, a rather strong (012) reflection is observed; apparently it is not associated with the inclusions of unoriented grains, for if this were so, the XRD pattern most likely would have featured (107), (114), and other strongest reflections [35]. The (012) reflection might arise from the part of the phase located in the blistering areas, where it is obviously impossible to maintain the same orientation as and in the defect-free areas of the film. Apart from the HF peaks, the XRD pattern features peaks due to titanium and titanium dioxide (rutile).

In the XRD pattern of the BaM/Ti/Si films, HF reflections were not found. As for BaM/Al_2O_3/Ti/Si, the (002) titanium peak and fewer TiO_2 reflections were observed here. Two additional peaks appeared in the 2θ range between 20° and 30°; they were assigned

Table 1. Assignment of XRD reflections in BaM/Ti/Si and BaM/Al_2O_3/Ti/Si samples

Phase	Peak position, deg	(*hkl*)
$BaFe_{12}O_{19}$	19.07	(012)
	23.33	(006)
	31.35	(008)
$BaFe_2O_4$	24.98	(022)
	28.12	(420)
	28.12	(412)
Ti	38.41	(002)
	62.94	(110)
TiO_2 (rutile)	27.48	(110)
	36.20	(101)
	39.41	(200)
	56.24	(220)
	62.94	(002)
Si	69.53	(004)

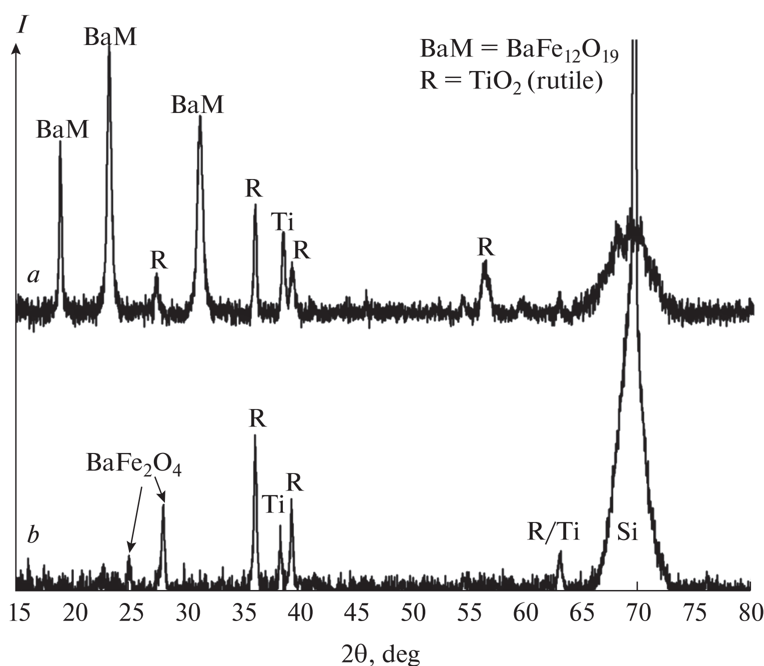

Fig. 2. X-ray diffraction patterns of (a) $BaM/Al_2O_3/Ti/Si$ and (b) BaM/Ti/Si samples.

to barium monoferrite $BaFe_2O_4$. It is obvious that the full formation of hexagonal barium ferrite did not occur; the only possible explanation to this is chemical interaction between the BaM film and the underlying layers. The formation of foreign phases in the BaM/Ti/Si sample explains its unusual surface morphology.

Thus, we may assume that $Al_2O_3/Ti/Si$ and Ti/Si structures are inapplicable for growing anisotropic hexaferrite films.

Nevertheless, understanding of stress formation processes in the prepared samples can help to reduce them through the implementation of certain technological operations. The greatest contribution to these processes is made by heat treatment, which changes the film volume. However, this change cannot be reduced to mere thermal expansion and the mismatch between the temperature coefficients of linear expansion (TCLEs). First, the HF crystallizes from the amorphous phase, as a result of which the atoms are ordered and, accordingly, the density (and volume) of the material changes. Secondly, when heated to 900°C, the Ti layer undergoes various phase transformations, either reversible ($\alpha \leftrightarrow \beta$ transition), or irreversible (oxygen diffusion and oxidation, crystallization of TiO_2 into anatase and rutile [36]). These processes induce stresses in the films and contribute to the formation of bulges. The pre-annealing of titanium films, which was carried out in the second phase of our study, can help to separate the time windows for phase transformation in BaM and TiO_2, to weaken their effects on the whole structure. It is assumed that titanium would be completely/partly oxidized upon heat treatment under air (900°C, 3 h), which would neutralize/reduce the contribution from α-Ti $\leftrightarrow$ β-Ti transformation. The anatase–rutile irreversible transition would end by this moment, and so would not cause an effect during the annealing. In addition, rutile and titanium have appreciably differing TCLEs [37, 38]. It follows that the stresses associated with the TCLE mismatch will appear in the TiO_2/Ti system upon cooling. The one who intends to assess the effect of these stresses on the state of the whole composite should be aware of the thickness of the oxidized titanium layer. From this point of view, it is obviously much easier to work with a single-phase TiO_2 layer. In view of the above, it looks quite reasonable to oxidize titanium. One sample was manufactured on oxidized silicon in order to provide an additional source of oxygen for TiO_2 formation. There are no prerequisites for the growth of anisotropic HF because of the polycrystalline state of TiO_2. Therefore, manufacturing of samples like $BaM/(TiO_2 + Ti)/Si(\text{or } SiO_2/Si)$ made no sense in the context of this work; an amorphous Al_2O_3 layer was used in all cases.

At the second stage of our study, additional attention was paid to the relief of the barrier layers (Fig. 3). We should mention the Al_2O_3 structure where rounded grains are morphologically close to (00l) BaM crystallites (Fig. 1 and the results from [30]). These data cast doubt on the amorphism of the Al_2O_3 coating; however, there are grounds to suggest that appreciable crystal ordering is yet not intrinsic to this phase. First, evidence comes from XRD patterns:

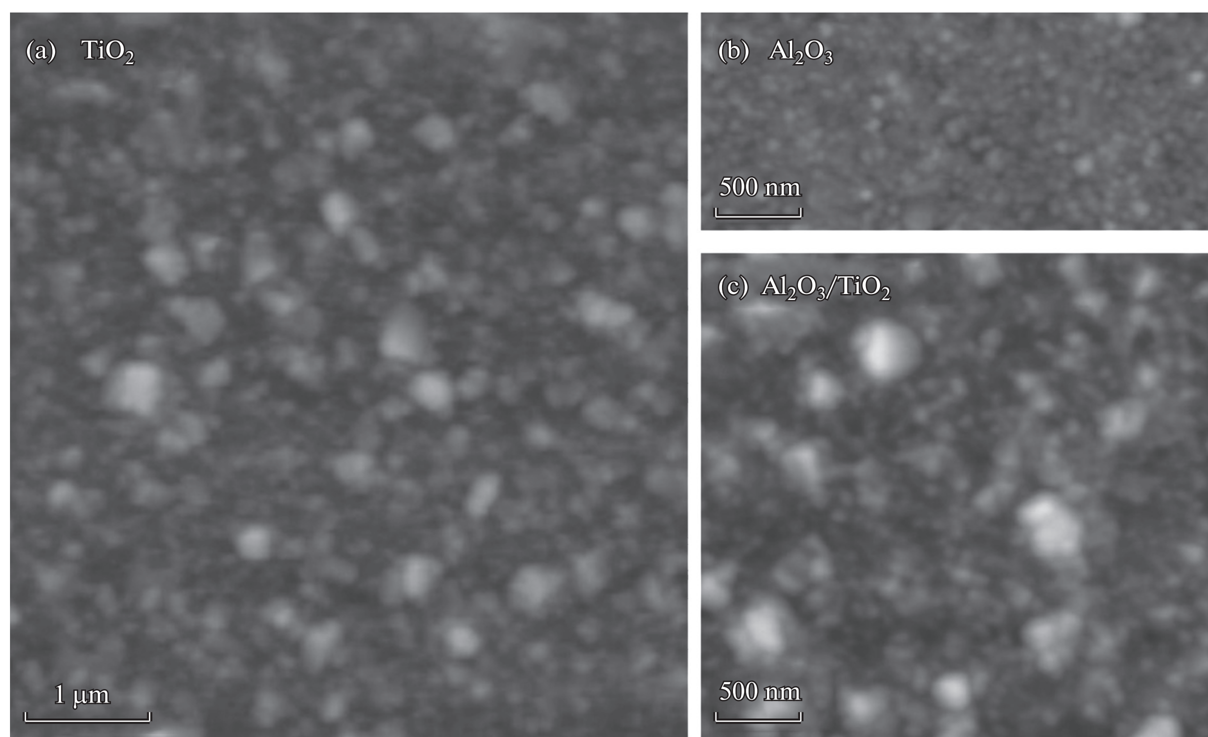

Fig. 3. AFM images of (a) TiO_2, (b) Al_2O_3, and (c) Al_2O_3 films on TiO_2.

Al_2O_3 peaks are unobserved, while the HF with a similar structure is unequivocally detected in the XRD pattern (both in this study and in [30]). Second, a similar globular structure of amorphous films was previously observed in other materials: in silicon oxide [39] and hematite [40].

Optical microscopy of the HF films manufactured at the second part of the study showed the absence of bulges or signs of their nucleation (Fig. 4), indicating the adequacy of the approach used. The results of AFM are mostly in line with expectations: HF grains have a rounded shape typical of (00l) texture. The SiO_2 layer does not have a significant effect on the BaM microstructure. Unusual large structures unobservable hitherto were found. Most likely, these inhomogeneities are associated with large protruding TiO_2 crystallites (Fig. 3a). It can be seen that the Al_2O_3 layer only partially smoothens the surface, "dulling" the TiO_2 grain faces (Fig. 3c). Probably, the HF film in a similar manner inherits the relief features of the lower layers.

Figure 5 shows the XRD patterns of the prepared samples, with peak assignment given in Table 2. Of the compounds of the Ba–Fe–O system, only the (00l) reflections of barium hexaferrite are observed; this is the most significant fact in the context of this work. The (002) titanium peak does not appear, nor any of its other reflections; this signifies that the Ti film is completely oxidized. Many of the remaining reflections are not identifiable unambiguously. However, there is

Table 2. Assignment of XRD patterns in $BaM/Al_2O_3/TiO_2/SiO_2/Si$ and $BaM/Al_2O_3/TiO_2/Si$ samples

Phase	Peak position, deg	(*hkl*)
$BaFe_{12}O_{19}$	23.37	(006)
	31.33	(008)
	39.53	(00<u>10</u>)
TiO_2 (rutile)	36.3	(101)
	54.65	(211)
	56.43	(220)
	76.42	(202)
	82.52	(321)
TiO_2 (brookite)	33.12	(020)
	54.65	(131)
	55.53	(421)
	56.43	(412)
	61.78	(502)
	65.97	(611)
	76.42	(432)
	82.52	(630)
SiO_2 (quartz)	56.43	(210)
	66.58	(212)
	76.42	(220)
	82.52	(311)
$TiAl_2O_5$	33.76	(023)
	47.84	(043)
	54.65	(220)
	61.78	(135)
	65.97	(241)
	76.42	(711)
	82.52	(810)
Si	69.53	(004)

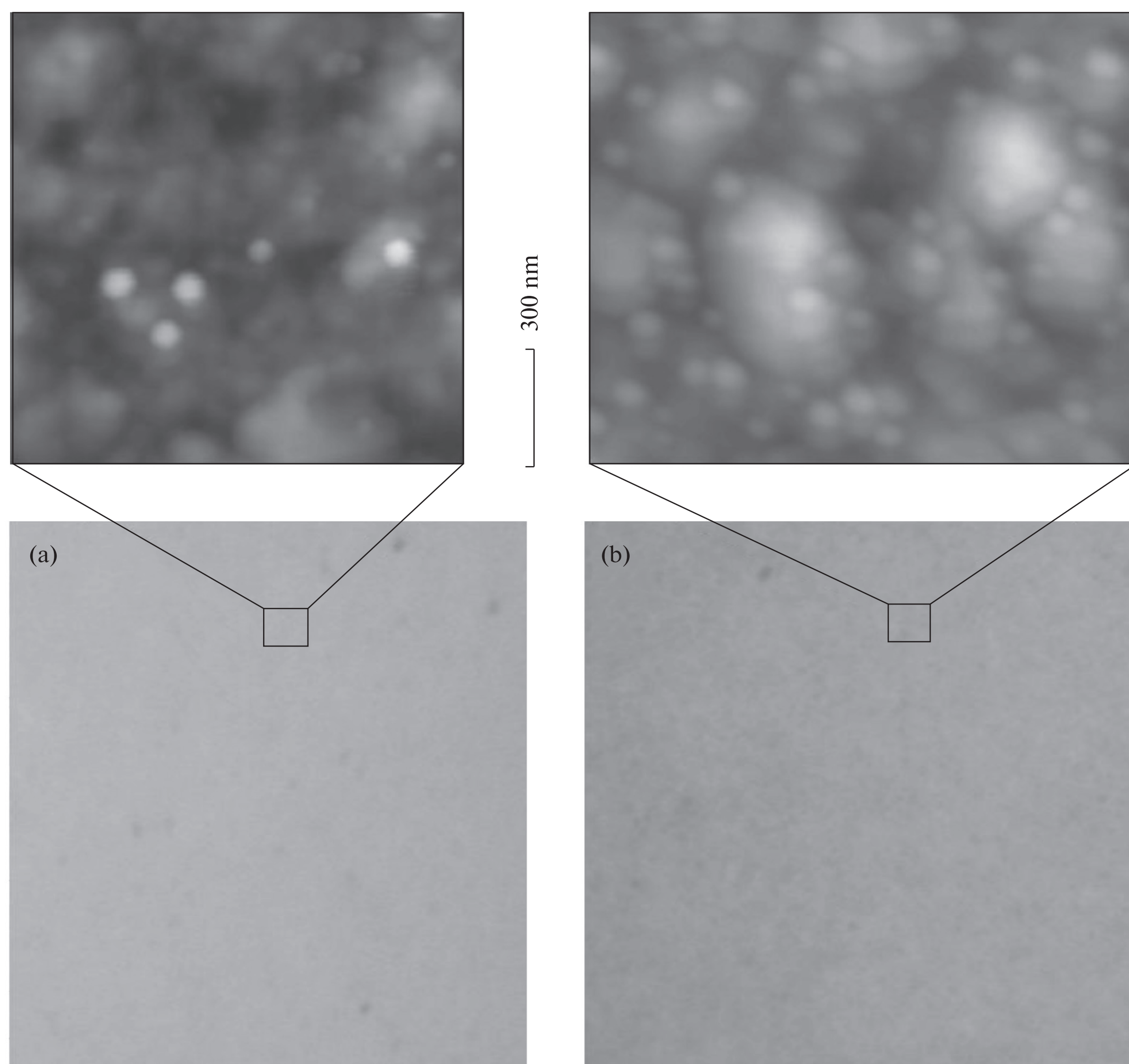

Fig. 4. Optical images (×20) and AFM images of (a) $BaM/Al_2O_3/TiO_2/SiO_2/Si$ and (b) $BaM/Al_2O_3/TiO_2/Si$ samples.

a high degree of probability that these peaks reflect the presence of Ti, Al, and Si oxides, which makes their detailed identification a matter of secondary importance. Of particular interest is the identity of XRD patterns of $BaM/Al_2O_3/TiO_2/Si$ and $BaM/Al_2O_3/TiO_2/SiO_2/Si$ samples (except for the differing backgrounds). Multiple reflections due to SiO_2 crystal inclusions were observed on the XRD patterns of (111) silicon oxidized at 1050°C [41]. Since in the work presented here silicon was oxidized at a higher temperature, SiO_2 reflections were also expected to appear. However, no peaks were observed in the positions directly identical to those observed in [41]. Some reflections may still be assigned to SiO_2, and the inconsistency of their positions with the previous observations [41] can arise from the different orientation of the silicon substrate used and, as a consequence, an alternative set of reflections of silicon oxide. Given this and the identity of XRD patterns of the samples, we may say that crystalline SiO_2 is present in $BaM/Al_2O_3/TiO_2/Si$, too. Silicon appears to be oxidized by the oxygen diffusing from TiO_2. For this process to occur, titanium oxide should be in contact with silicon, which is in good agreement with XRD data: At the first stage of the study, a coating of pure Ti is preserved and inhibits the access of oxygen to the substrate, due to which SiO_2 peaks are unobserved; at the second stage, the Ti completely converts to TiO_2, and silicon oxidation in the described route is possible. One more specific feature of the XRD patterns of prepared samples is that most TiO_2 is brookite. As a rule, brookite is considered less stable than rutile [42]. Like the anatase-to-rutile transformation, the brookite-to-rutile transformation is irreversible. Nevertheless, this

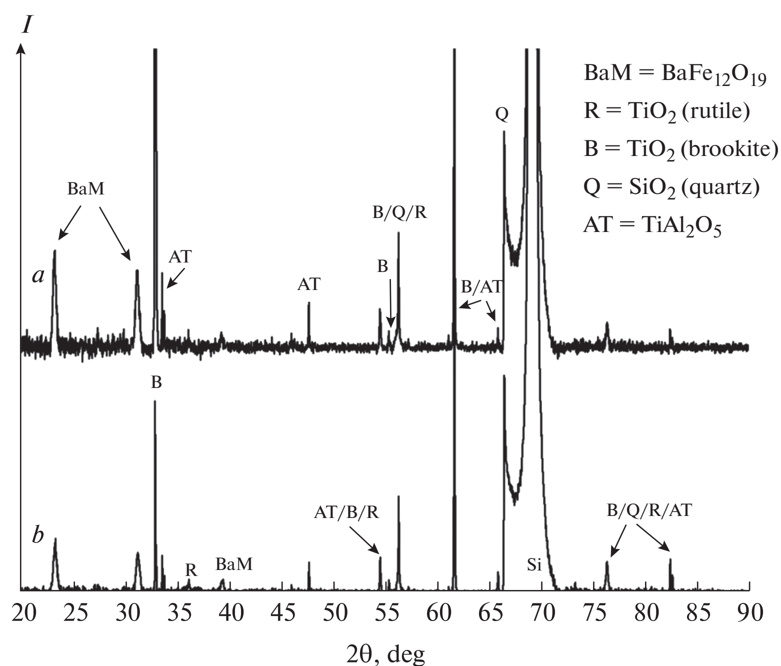

Fig. 5. X-ray diffraction patterns of (*a*) $BaM/Al_2O_3/TiO_2/SiO_2/Si$ and (*b*) $BaM/Al_2O_3/TiO_2/Si$ samples.

phase transition proceeds gradually and takes hours even at 900°C [43, 44]; from this, it is clear why the transformation in these samples did not go to completion. Nevertheless, it is unclear why this polymorph was formed in the films of the second stage and was absent at the first stage. As a rough approximation, this can be attributed to the titanium oxidation conditions. Mangum et al. [45] showed that what polymorph is formed in TiO_2 films depends on oxygen access, which is obviously different during annealing of Ti/Si and $BaM/Al_2O_3/Ti/Si$. It seems that aluminum titanate $TiAl_2O_5$ is also present in the films; it can in principle form at 900°C [46]. Apparently, titanate was not observed at the first stage of the study; its formation requires a larger amount of TiO_2 or depends on its polymorph. At any rate, the particular phases formed in the Al–Ti–O system are beyond the scope of this study, since it focuses on hexaferrite films. Nevertheless, since the interaction of $BaFe_{12}O_{19}$ with $TiAl_2O_5$ has not been studied, the depletion of the Al_2O_3 layer due to its reaction with TiO_2 raises some doubts about the suitability of such coatings for growing hexaferrite. On the other hand, aluminum titanate is known for its low thermal expansion and high temperature resistance [47], and these properties could give an additional reduction in stress.

CONCLUSIONS

Textured barium hexaferrite films have been grown on $Al_2O_3/TiO_2(Ti)/Si$ substrates. The TiO_2 (Ti) layer in this structure performs as a silicon diffusion barrier, and Al_2O_3, being an amorphous surface, contributes to the spontaneous formation of the hexaferrite texture. Hexaferrite formation when $BaFe_{12}O_{19}$ and TiO_2/Ti are in a direct contact is not confirmed by X-ray powder diffraction. When $Al_2O_3/TiO_2/Ti$ is used, phase transformations in titanium and titanium dioxide induce a change in film volume upon annealing, and strong stresses are induced to generate macroscopic defects. This problem has been eliminated by pre-oxidation of titanium films, but a $TiAl_2O_5$ phase was detected in $BaM/Al_2O_3/TiO_2$ samples; so, the interaction of this phase with the hexaferrite needs to be studied. Despite this, $BaFe_{12}O_{19}$ films on $Al_2O_3/TiO_2/Si$ have high degrees of texture as probed by XRD and AFM. Therefore, they have a potential for use, with a greater hexaferrite layer thickness, in planar microwave devices for the millimeter wavelength range and terahertz spectroscopy.

CONFLICT OF INTEREST

The authors declare that they have no conflicts of interests.

REFERENCES

1. R. C. Pullar, Prog. Mater. Sci. **57**, 1191 (2012). https://doi.org/10.1016/j.pmatsci.2012.04.001
2. C. Fernandez De Julian, C. Sangregorio, J. de la Figuera, et al., J. Phys. D: Appl. Phys. **54**, 153001 (2021). https://doi.org/10.1088/1361-6463/abd272

3. R. Jotania, AIP. Conf. Proc. **1621**, 596 (2014). https://doi.org/10.1063/1.4898528
4. V. G. Kostishin, D. N. Chitanov, A. G. Nalogin, et al., Russ. J. Inorg. Chem. **61**, 279 (2016). https://doi.org/10.1134/S0036023616030116
5. V. V. Korovushkin, A. V. Trukhanov, M. N. Shipko, et al., Russ. J. Inorg. Chem. **64**, 574 (2019). https://doi.org/10.1134/S0036023619050115
6. V. V. Korovushkin, A. V. Trukhanov, V. G. Kostishin, et al., Phys. Solid State **62**, 891 (2020). https://doi.org/10.1134/S1063783420050145
7. H. Li, L. Zheng, D. Deng, et al., J. Alloys Compd. **862**, 158638 (2021). https://doi.org/10.1016/j.jallcom.2021.158638
8. H. K. Satyapal, R. K. Singh, S. S. Kumar, et al., Mater. Today Proc. **44**, 1833 (2021).
9. K. S. Martirosyan, E. Galstyan, S. M. Hossain, et al., Mater. Sci. Eng. B **176**, 8 (2011). https://doi.org/10.1016/j.mseb.2010.08.005
10. V. K. Chakradhary and M. J. Akhtar, Composites B **183**, 107667 (2020). https://doi.org/10.1016/j.compositesb.2019.107667
11. X. Zhang, Y. Zhang, S. Cao, et al., Mater. Lett. **248**, 24 (2019). https://doi.org/10.1016/j.matlet.2019.03.139
12. B. K. O'Neil and J. L. Young, *IEEE Antennas and Propagation Society International Symposium,* San Diego, 2008. https://doi.org/10.1109/APS.2008.4619493
13. S. G. Wang, S. D. Yoon, and C. Vittoria, J. Appl. Phys. **92**, 6728 (2002). https://doi.org/10.1063/1.1517749
14. E. D. Solovyova, M. L. Calzada, and A. G. Belous, J. Sol-Gel Sci. Technol. **75**, 215 (2015). https://doi.org/10.1007/s10971-015-3692-6
15. H. Tang, W. Zhang, B. Peng, and W. Zhang, Thin Solid Films **518**, 3342 (2010). https://doi.org/10.1016/j.tsf.2010.01.038
16. S. Yong An, S. Won Lee, I.-B. Shim, and C. Sung Kim, Phys. Status Solidi A **189**, 893 (2002). https://doi.org/10.1002/1521-396X(200202)189:3<893::AID-PSSA893>3.0.CO;2-O
17. S. Verma, S. Mahadevan, C. Pahwa, et al., J. Supercond. Nov. Magn. **33**, 2507 (2020). https://doi.org/10.1007/s10948-020-05494-2
18. C. Velez, J. Ewing, S. Hwangbo, et al., *EEE MTT-S International Microwave Workshop Series on Advanced Materials and Processes for RF and THz Applications (IMWS-AMP), Ann Arbor*. Michigan, 16–18 July 2018. https://doi.org/10.1109/IMWS-AMP.2018.8457152
19. S. M. Masoudpanah, S. A. Seyyed Ebrahimi, and C. K. Ong, J. Magn. Magn. Mater. **324**, 2894 (2012). https://doi.org/10.1016/j.jmmm.2012.04.034
20. Z. Xu, Z. Lan, K. Sun, et al., J. Alloys Compd. **575**, 257 (2013). https://doi.org/10.1016/j.jallcom.2013.04.084
21. V. G. Kostishin, A. Yu. Mironovich, R. I. Shakirzyanov, et al., Usp. Prikl. Fis. **8**, 370 (2020).
22. S. M. Masoudpanah, S. A. Seyyed Ebrahimi, and C. K. Ong, J. Magn. Magn. Mater. **324**, 2654 (2012). https://doi.org/10.1016/j.jmmm.2012.03.040
23. Z. Xu, Z. Lan, K. Sun, et al., Appl. Surf. Sci. **271**, 362 (2013). https://doi.org/10.1016/j.apsusc.2013.01.203
24. F. M. Mwema, O. P. Oladijo, S. A. Akinlabi, and E. T. Akinlabi, J. Alloys Compd. **747**, 306 (2018). https://doi.org/10.1016/j.jallcom.2018.03.006
25. A. M. Glezer and N. A. Shurygina, *Amorphous Nanocrystalline Alloys* (Fizmatlit, Moscow, 2013) [in Russian].
26. N. N. Shams, M. Matsumoto, and A. Morisako, IEEE Trans. Magn. **40**, 2955 (2004). https://doi.org/10.1109/TMAG.2004.829276
27. A. Morisako, N. N. Shams, Y. Miura, et al., J. Magn. Magn. Mater. **272–276**, 2191 (2004). https://doi.org/10.1016/j.jmmm.2003.12.632
28. P. Kulik, C. Yu, and A. Sokolov, Scr. Mater. **188**, 190 (2020). https://doi.org/10.1016/j.scriptamat.2020.07.041
29. V. V. Pan'kov, A. I. Stognii, V. D. Koshevar, and V. A. Ketsko, Inorg. Mater. **44**, 1022 (2008). https://doi.org/10.1134/S0020168508090203
30. V. G. Kostishin, A. Y. Mironovich, A. V. Timofeev, et al., Russ. J. Inorg. Chem. **66**, 603 (2021). https://doi.org/10.1134/S003602362104015X
31. G. Abadias, E. Chason, J. Keckes, et al., J. Vac. Sci. Technol. A **36**, 020801 (2018). https://doi.org/10.1116/1.5011790
32. W. Jiang, D. Xu, S. Yao, et al., Mater. Sci. Semicond. Proc. **43**, 222 (2016). https://doi.org/10.1016/j.mssp.2015.12.020
33. D. Dergez, J. Schalko, A. Bittner, and U. Schmid, Appl. Surf. Sci. **284**, 348 (2013). https://doi.org/10.1016/j.apsusc.2013.07.104
34. V. Chawla, R. Jayaganthan, A. K. Chawla, and R. Chandra, Mater. Chem. Phys. **111**, 414 (2008). https://doi.org/10.1016/j.matchemphys.2008.04.048
35. W. D. Townes, J. H. Fang, and A. J. Perrotta, Z. Kristallogr. **125**, 437 (1967). https://doi.org/10.1524/ZKRI.1967.125.125.437
36. E. Gemelli and N. H. A. Camargo, Revista Materia **12**, 525 (2007). https://doi.org/10.1590/S1517-70762007000300014
37. D. V. Pavlenko, D. V. Tkach, S. M. Danilova-Tretyak, and L. E. Evseeva, J. Eng. Phys. Thermophys. **90**, 685 (2017). https://doi.org/10.1007/s10891-017-1616-8
38. R. K. Kirby, J. Res. Natl. Bur. Stand. A: Phys. Chem. **71**, 363 (1967). https://dx.doi.org/10.6028%2Fjres.071A.041

39. V. A. Fedorov, A. D. Berezner, A. I. Beskrovnyi, et al., Phys. Solid State **60**, 705 (2018). https://doi.org/10.1134/S1063783418040091
40. V. Yu. Kolosov, K. L. Shvamm, R. V. Gainutdinov, and A. L. Tolstikhina, Bull. Russ. Acad. Sci. Phys. **71**, 1442 (2007). https://doi.org/10.3103/S1062873807100280
41. V. G. Kostishin, A. Yu. Mironovich, A. V. Timofeev, et al., Semiconductors **55**, 308 (2021). https://doi.org/10.1134/S106378262103012X
42. E. P. Lokshin and T. A. Sednev, Russ. J. Gen. Chem. **81**, 1749 (2011). https://doi.org/10.1134/S1070363211090015
43. J. Huberty and H. Xu, J. Solid State Chem. **181**, 508 (2008). https://doi.org/10.1016/j.jssc.2007.12.015
44. M. P. Gonullu and H. Ates, Superlattices Microstruct. **147**, 106699 (2020). https://doi.org/10.1016/j.spmi.2020.106699
45. J. S. Mangum, O. Agirseven, J. E. S. Haggerty, et al., J. Non-Cryst. Solids **505**, 109 (2019). https://doi.org/10.1016/j.jnoncrysol.2018.10.049
46. A. Azarniya, A. Azarniya, H. R. M. Hosseini, and A. Simchi, Mater. Charact. **103**, 125 (2015). https://doi.org/10.1016/j.matchar.2015.03.030
47. Y. Ohya, S. Yamamoto, T. Ban, et al., J. Eur. Ceram. Soc. **37**, 1673 (2017). https://doi.org/10.1016/j.jeurceramsoc.2016.11.037

Translated by O. Fedorova